

# Crystal structure determination and inhibition studies of a novel xylanase and $\alpha$ -amylase inhibitor protein (XAIP) from *Scadoxus multiflorus*

Sanjit Kumar, Nagendra Singh, Mau Sinha, Divya Dube, S. Baskar Singh, Asha Bhushan, Punit Kaur, Alagiri Srinivasan, Sujata Sharma and Tej P. Singh

Department of Biophysics, All India Institute of Medical Sciences, New Delhi, India

## Keywords

crystal structure; enzyme inhibition; TIM barrel fold; xylanase;  $\alpha$ -amylase

## Correspondence

T. P. Singh, Department of Biophysics, All India Institute of Medical Sciences, Ansari Nagar, New Delhi – 110 029, India  
Fax: +91 11 2658 8663  
Tel: +91 11 2658 8931  
E-mail: tpsingh.aiims@gmail.com

## Database

The complete nucleotide and derived amino acid sequences of XAIP are available in the EMBL/GenBank/DDJB databases under the accession number EU663621  
Structural data are available in the Protein Data Bank database under the accession numbers 3HU7 and 3M7S.

(Received 18 March 2010, revised 27 April 2010, accepted 29 April 2010)

doi:10.1111/j.1742-4658.2010.07703.x

A novel plant protein isolated from the underground bulbs of *Scadoxus multiflorus*, xylanase and  $\alpha$ -amylase inhibitor protein (XAIP), inhibits two structurally and functionally unrelated enzymes: xylanase and  $\alpha$ -amylase. The mature protein contains 272 amino acid residues which show sequence identities of 48% to the plant chitinase hevamine and 36% to xylanase inhibitor protein-I, a double-headed inhibitor of GH10 and GH11 xylanases. However, unlike hevamine, it is enzymatically inactive and, unlike xylanase inhibitor protein-I, it inhibits two functionally different classes of enzyme. The crystal structure of XAIP has been determined at 2.0 Å resolution and refined to  $R_{\text{cryst}}$  and  $R_{\text{free}}$  factors of 15.2% and 18.6%, respectively. The polypeptide chain of XAIP adopts a modified triosephosphate isomerase barrel fold with eight  $\beta$ -strands in the inner circle and nine  $\alpha$ -helices forming the outer ring. The structure contains three *cis* peptide bonds: Gly33–Phe34, Tyr159–Pro160 and Trp253–Asp254. Although hevamine has a long accessible carbohydrate-binding channel, in XAIP this channel is almost completely filled with the side-chains of residues Phe13, Pro77, Lys78 and Trp253. Solution studies indicate that XAIP inhibits GH11 family xylanases and GH13 family  $\alpha$ -amylases through two independent binding sites located on opposite surfaces of the protein. Comparison of the structure of XAIP with that of xylanase inhibitor protein-I, and docking studies, suggest that loops  $\alpha$ 3– $\beta$ 4 and  $\alpha$ 4– $\beta$ 5 may be involved in the binding of GH11 xylanase, and that helix  $\alpha$ 7 and loop  $\beta$ 6– $\alpha$ 6 are suitable for the interaction with  $\alpha$ -amylase.

## Introduction

In order to protect themselves against attack by cell wall-degrading enzymes secreted by plant pathogens, plants produce a vast array of inhibitors of pectinolytic enzymes [1–3]. A few structures of such proteins have been determined, but newer and more potent proteins with multiple binding properties are being identified regularly [4–8]. Initially, these protein inhibitors were

considered to have been part of the original composition of plant proteins to protect against their own enzymes, but, subsequently, they seem to have evolved through induction to fight against new and emerging pathogens. Detailed binding studies and three-dimensional structural determinations of these new proteins will provide useful insights into their functional

## Abbreviations

BASI, barley  $\alpha$ -amylase/subtilisin inhibitor; Con-B, concanavalin-B; GH, glycosyl hydrolase; TIM, triosephosphate isomerase; XAIP, xylanase and  $\alpha$ -amylase inhibitor protein; XIP-I, xylanase inhibitor protein-I.

properties and structure–function relationships. Therefore, it is of utmost importance to understand how proteins with significant sequence identities and structural similarities evolve to perform different functions. A double-headed inhibitor of GH10 and GH11 xylanases (xylanase inhibitor protein-I, XIP-I) is a good example, as it shows a strong structural resemblance to one of the enzymes whose function it inhibits. It folds into a triosephosphate isomerase (TIM) barrel structure and inhibits the functions of GH10 xylanase with a TIM barrel fold and GH11 xylanase with a jelly roll conformation [9]. In the present context, it is important to understand the components of molecular design for correlation with new functions. In order to recognize the specificities and patterns of protein–protein interactions in these systems, it is necessary to determine the three-dimensional structures of individual proteins and their complexes. We have isolated a novel plant protein from *Scadoxus multiflorus* and found that it binds specifically to two structurally very different enzymes, GH11 xylanase and GH13  $\alpha$ -amylase, resulting in the inhibition of their enzymatic actions. Thus, this protein is referred to here as ‘xylanase and  $\alpha$ -amylase inhibitor protein’ (XAIP). Its complete amino acid sequence and three-dimensional structure have been determined. As a member of the hydrolase 18C family, it shows sequence identities of 48%, 39% and 11% with hevamine [10], concanavalin-B (Con-B) [11] and narbonin [12], respectively. The functions of the last two enzymes are still unknown. It also shows sequence identity of 36% with XIP-I [9,13]. The structural determination of XAIP has revealed that its polypeptide chain adopts an overall TIM barrel conformation, similar to that reported for other family 18 glycosyl hydrolases (GHs) [14]. However, notably, this structure contains an extra helix,  $\alpha 8'$ , which is located between  $\beta$ -strand  $\beta 8$  and  $\alpha$ -helix  $\alpha 8$ , indicating that this protein belongs to the subgroup of family 18C proteins [15]. The structure also showed that the carbohydrate-binding channel in XAIP is filled with the side-chains of several amino acid residues, and hence not accessible for the binding of carbohydrates.

## Results

### Sequence analysis

The complete nucleotide and derived amino acid sequences of XAIP have been determined and deposited in the GenBank/EMBL data libraries under accession number EU663621. XAIP consists of 272 amino acid residues, including four cysteines linked by two disulfide bridges: Cys22–Cys63 and Cys157–Cys186.

A multiple sequence alignment shows that XAIP shares sequence identities of 48%, 39%, 36% and 11% with hevamine [10], Con-B [11], XIP-I [9,13] and narbonin [12], respectively (Fig. 1). The chain lengths of these proteins range from 272 to 299 residues. The disulfide linkages in XAIP are identical to those of XIP-I [9,13], whereas hevamine and Con-B have six cysteine residues in each with an additional disulfide bridge: Cys50–Cys57 (Fig. 1). Narbonin has only one cysteine residue in the C-terminal region. Hevamine shows chitinase activity with active site residues Asp125, Glu127 and Tyr183 (hevamine numbering). The corresponding triads in XAIP, Con-B, narbonin and XIP-I are His123, Glu125, Tyr181; Asp129, Gln131, Tyr189; His130, Glu132, Gln191; and Phe123, Glu125, Tyr181, respectively, indicating that all lack the standard combination of residues for chitin hydrolysing activity.

### XAIP lacks chitin hydrolysing activity

The comparison of the amino acid sequence of XAIP with that of hevamine shows that XAIP also belongs to the GH family 18C proteins. The active site triads in hevamine [10] and bacterial chitinase [16] contain residues Asp125, Glu127 and Tyr183, whereas the corresponding residues in XAIP are His123, Glu125 and Tyr181, indicating a change from Asp to His in XAIP. In order to determine experimentally the chitinase activity of XAIP, a chitinolytic assay was carried out at pH 8.0 using chitin azure (chitin dyed with Remazol Brilliant violet [17]) as the substrate. When chitin dyed with Remazol Brilliant violet was hydrolysed with chitinase, absorption was observed at 575 nm. The optical densities for the product samples obtained by the reaction of chitinase with chitin azure clearly showed a distinct maximum at 575 nm. A similar reaction set-up with XAIP did not show an absorption maximum at 575 nm. As shown in Fig. 2, at 575 nm for samples with chitinase, a large absorption maximum was observed, whereas, with XAIP and without any protein in the experimental samples, there were no changes in absorption, indicating that XAIP does not possess chitinase-like chitinolytic activity.

### Inhibition of amylase and xylanase

As XAIP shows significant sequence identity and considerable structural similarity with XIP-I [9,13], which is an inhibitor of GH10 and GH11 xylanases, the role of XAIP as an inhibitor of various pathogen enzymes associated with plants, such as xylanases, chitinases

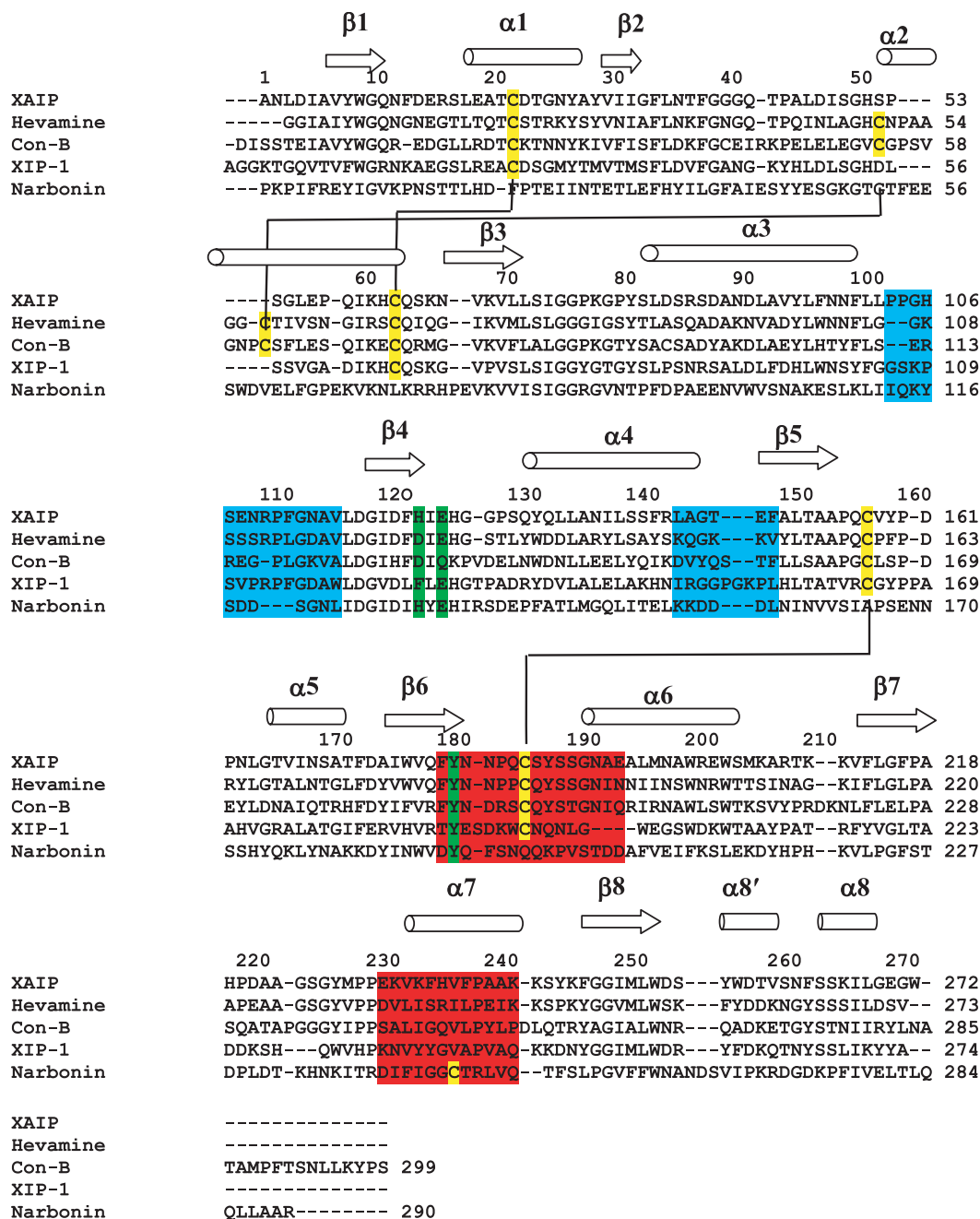


**Fig. 1.** Sequence alignment of XAIP (EU 663621), XIP-1 [9,13], hevamine [10], Con-B [11] and narbonin [12]. Secondary structural elements, i.e.  $\alpha$ -helices and  $\beta$ -strands, are represented by cylinders and arrows, respectively. The cysteines are shown in yellow and disulfide bridges are indicated by connecting links. The regions of the polypeptide chain involved in the binding site with GH11 xylanase are shown on a blue background and those with  $\alpha$ -amylase are shown on a red background. The amino acids corresponding to the chitinase active site are indicated on a green background.

and  $\alpha$ -amylases, was examined. The results of inhibition assays showed that, in the presence of XAIP, the activities of  $\alpha$ -amylase from *Bacillus licheniformis* [18] and xylanase from fungus *Penicillium funiculosum* [9] of family GH11 were inhibited considerably. The

inhibition of GH11 xylanase was recorded to be up to 50% for an enzyme to XAIP molar ratio of 1 : 1.5 (Fig. 3B). Similarly, at a molar ratio of 1 : 1.2 between  $\alpha$ -amylase and XAIP, the activity of  $\alpha$ -amylase was reduced to about 50% (Fig. 3A). The  $IC_{50}$  values for

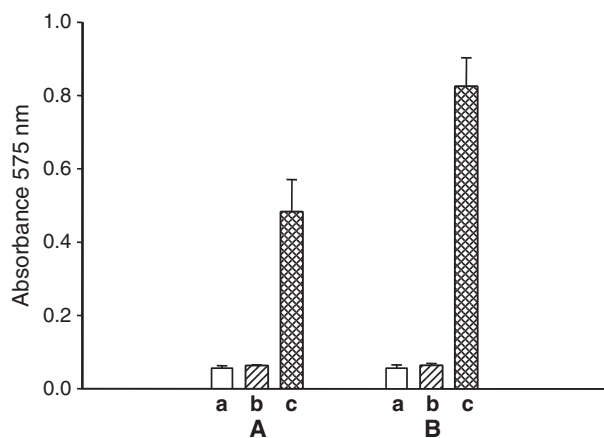


**Fig. 2.** Measurements of chitinolytic activity of XAIP using chitin azure (A) in the absence of any protein (a), with 1  $\mu\text{M}$  concentration of XAIP (b) and with 1  $\mu\text{M}$  concentration of chitinase enzyme (c) for 2 h, and (B) in the absence of any protein (a), with 100  $\mu\text{M}$  concentration of XAIP (b) and with 100  $\mu\text{M}$  concentration of chitinase enzyme (c) for 4 h. After 4 h, no change was observed.

enzymes GH11 xylanase and  $\alpha$ -amylase with XAIP were calculated to be 3.0 and 2.4  $\mu\text{M}$ , respectively.

### Evidence of complex formation by gel filtration

The gel filtration profiles for the mixtures of XAIP and GH11 xylanase and XAIP and GH13  $\alpha$ -amylase were analysed. The prominent peaks corresponding to complexes of XAIP with GH11 xylanase and GH13  $\alpha$ -amylase were observed in each case. Two lower molecular weight minor peaks were also detected in both cases. The results of the third experiment, when all three proteins XAIP, GH11 xylanase and GH13  $\alpha$ -amylase, were mixed, showed a significant peak corresponding to the molecular weight of the ternary complex of XAIP, GH11 xylanase and GH13  $\alpha$ -amylase. These observations indicate that XAIP associates with GH11 xylanase and GH13  $\alpha$ -amylase, as well as with both xylanase and  $\alpha$ -amylase simultaneously.

### Tissue distribution of XAIP

The output of SDS-PAGE for the samples obtained from germinated bulb, root, leaf and flower showed an intense band for XAIP (as confirmed by N-terminal sequence determination) in the germinated bulb samples, but the corresponding band was absent in the leaf and flower samples, whereas, in the root sample, a very thin band of XAIP was visible. The enzyme inhibition assay using GH11 xylanase and GH13  $\alpha$ -amylase showed maximum inhibitory effects for the

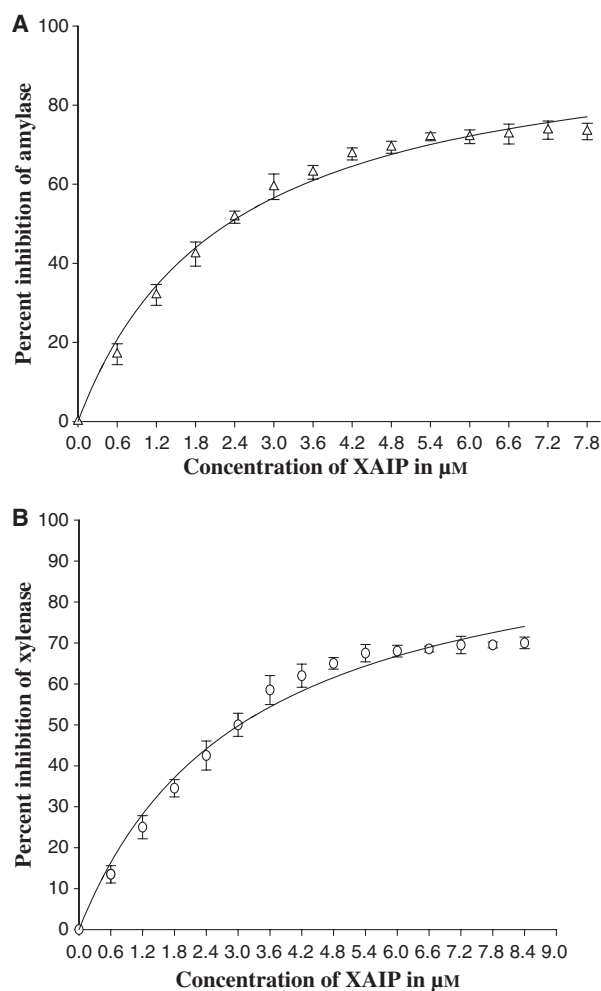


**Fig. 3.** Inhibition of GH11 xylanase from *Penicillium furniculosum* with increasing concentrations of XAIP (A) and of  $\alpha$ -amylase from *Bacillus licheniformis* with increasing concentrations of XAIP (B).

germinated bulb sample, whereas no inhibition was observed for leaf and flower samples, and mild inhibition for the root sample. These results clearly indicate that the tissue distributions and concentrations of XAIP are highest in germinated bulbs. XAIP is also present in the root, but at a relatively low concentration. In other tissues, such as leaf and flower, XAIP was not detected even after silver staining. Therefore, it is either absent or is present at an extremely low concentration. A similar distribution has also been reported in the case of XIP-I [19]. It is also noteworthy that, according to the classification of subcellular locations, XAIP is classified to be an extracellular secretory protein, as predicted using its amino acid sequence with the help of various procedures and software packages BACELLO [20], CELLO [21] and PROT COMP VERSION 6.0 [22].

### Quality of the model

The overall geometry of the crystallographically determined XAIP model at 2.0 Å resolution is excellent, as shown by continuous electron density for the polypeptide chain, as well as by the molprobity score of 84 percentile [23]. There is only one segment consisting of residues Pro103–Phe112 for which a slightly weak electron density was observed, although there was no ambiguity in tracing the protein chain or in the identification of side-chains, even though the value of the average *B* factor for the residues of this loop is higher ( $\sim 45 \text{ \AA}^2$ ) than the average *B* factor for the rest of the protein ( $23 \text{ \AA}^2$ ). The *B* values for the residues in this loop increase gradually as we move away from the two rigid ends at Pro103–Pro104 and Pro111–Phe112. The final model consists of 2108 protein atoms from 272 amino acid residues, one acetate and one phosphate ion, and 300 water oxygen atoms. The final values for the  $R_{\text{cryst}}$  and  $R_{\text{free}}$  factors are 15.1% and 18.6%, respectively. The rmsd values from ideality for bond lengths and angles are 0.01 Å and 1.8°, respectively. A Ramachandran plot [24] for the whole molecule shows 88.5% of residues in the most favoured regions, whereas 10.6% are observed in the additionally allowed regions. Only two residues, His106 and

Ser130, have  $\phi$ ,  $\psi$  angles in the generously allowed region, as defined by PROCHECK [25], whereas no residue falls in the disallowed regions. There are three *cis* peptides between Gly33–Phe34, Tyr159–Pro160 and Trp253–Asp254 which are conserved in the structures of other members of the subgroup consisting of hevamine [10], Con-B [11], narbonin [12] and XIP-I [9,13].

### Overall structure of XAIP

The polypeptide chain of XAIP folds into an elliptical TIM barrel structure with an eight-stranded parallel  $\beta$ -barrel in the centre surrounded by nine  $\alpha$ -helices (Fig. 4A). The observed TIM barrel structure of XAIP is similar to the classical  $(\beta/\alpha)_8$  barrel, except that it contains an extra  $\alpha$ -helix,  $\alpha 8'$ , between strand  $\beta 8$  and  $\alpha$ -helix  $\alpha 8$ . The helix  $\alpha 8'$  is also observed in hevamine [10], Con-B [11], narbonin [12] and XIP-I [9,13]. All of these proteins with an extra helix  $\alpha 8'$  are clubbed into a single subgroup, called family 18C proteins. As shown in Fig. 4A, the parallel  $\beta$ -strands from  $\beta 1$  to  $\beta 8$  form a continuous circumference of the internal barrel. In contrast, the surrounding  $\alpha$ -helices of the outer ring show gaps between various helices. The most prominent gap is observed between helices  $\alpha 2$  and  $\alpha 3$ . Interestingly, the C-terminal end of helix  $\alpha 3$  is abruptly

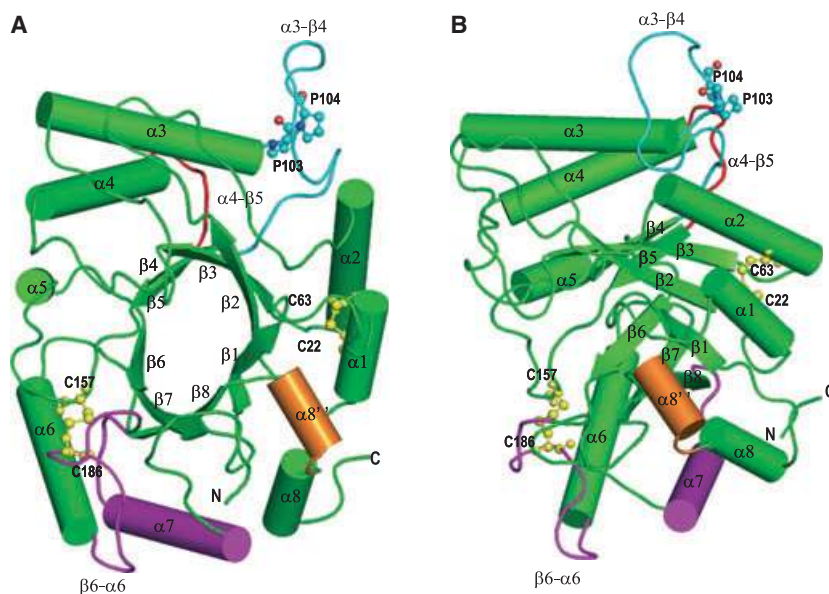


**Fig. 4.** Schematic representations of the structure of XAIP: (A) top view; (B) view after rotation by 90° along the vertical axis and 30° along the horizontal axis. The  $\alpha$ -helices (green) and  $\beta$ -strands (green) are labelled from 1 to 8. Two disulfide bonds are indicated in yellow. The additional  $\alpha$ -helix  $\alpha 8'$  is shown in orange. The loops  $\alpha 3$ – $\beta 4$  and  $\alpha 4$ – $\beta 5$  form the surface involved in binding with GH11 xylanase, and are shown in blue, whereas helix  $\alpha 7$  and loop  $\beta 6$ – $\alpha 6$  from the opposite surface of the protein are assumed to be involved in binding with  $\alpha$ -amylase, and are indicated in magenta. Residues Pro103–Pro104 are shown in a ball and stick representation. The figure was drawn using PYMOL [42].

interrupted because of the insertion of two Pro residues: Pro103 and Pro104. This loop is present at one end of the longest axis of the elliptical molecule (Fig. 4B). It is clear from the structure that the presence of two consecutive Pro residues at positions 103 and 104 alters the path of the protein chain, resulting in the formation of a loop that protrudes away from the protein surface into the solvent. There is yet another interesting feature of the XAIP structure which is related to the conformation of loop  $\beta_3$ - $\alpha_3$ . This loop extends via the centre of the inner  $\beta$ -barrel with Pro77 positioned at the centre of the  $\beta$ -barrel, thus reducing the internal space of the TIM barrel considerably. Of the three observed *cis* peptides, two (Gly33-Phe34 and Trp253-Asp254) are found at the ends of  $\beta$ -strands  $\beta_2$  and  $\beta_8$ , respectively. These are part of the inner TIM barrel wall, whereas the third *cis* peptide, Tyr159-Pro160, belongs to the short  $\beta_5$ - $\alpha_5$  loop on the surface of the protein. Both Tyr159 and Pro160 are part of the reverse  $\gamma$ -turn and are located in a tightly organized environment as a useful structural element. All three *cis* peptides are conserved in family 18C proteins. The single-domain TIM barrel structure of XAIP resembles closely those of hevamine, Con-B, XIP-I and narbonin. The average rms shifts for C $\alpha$  atoms of XAIP, when superimposed on those of hevamine, Con-B, XIP-I and narbonin, are 1.0 Å (256 residues), 1.1 Å (232 residues), 1.3 Å (228 residues) and 2.2 Å (185 residues), respectively.

### XAIP characteristic loop

The structural determination of XAIP revealed the presence of a novel loop that protrudes sharply away from the surface of the protein. The longest helix  $\alpha_3$  in the structure is terminated abruptly by the introduction of two consecutive Pro residues: Pro103 and Pro104. The presence of a Pro-Pro dipeptide is unique to the XAIP sequence as the residues at the corresponding positions in hevamine and Con-B are absent, whereas narbonin and XIP-I have residues other than Pro. The loop  $\alpha_3$ - $\beta_4$ , consisting of polypeptide segment Pro103-Phe112, protrudes outwardly from the body of the protein molecule (Fig. 4). However, this flexible loop is tightly anchored at the two rigid ends containing Pro103-Pro104 on one side and Pro111-Phe112 on the other. The lower part of the loop, which is proximal to the protein surface, is further stabilized by two hydrogen bonds involving NH1 and NH2 of the guanidinium group of Arg110 with the backbone carbonyl oxygen atom of Leu102. The anchoring on the C-terminal side of the loop is also strengthened by a tight type II'  $\beta$ -turn involving tetra-

peptide Phe112-Gly113-Asn114-Ala115. The firmly held loop at the two ends is very flexible in the middle as no other parts of the protein chain interact with the residues of this loop and, also, no other intraloop interactions are observed. The side-chains of residues His106, Ser107, Glu108 and Asn109 protrude away from the protein, presumably to form intermolecular interactions. In contrast, the corresponding segments in hevamine, Con-B and narbonin are flat relative to that of XAIP. In the case of XIP-I, the corresponding loop differs considerably in amino acid sequence, indicating a preference for a different recognition site.

### Carbohydrate recognition site

As the amino acid sequence and scaffolding of the polypeptide chain indicate that XAIP belongs to family 18C proteins to which catalytically active hevamine also belongs, the carbohydrate-binding site in XAIP was examined and compared with those of other carbohydrate-binding TIM barrel proteins. It has already been reported that both Con-B and narbonin can only bind small fragments of chitin polymers and are unable to hydrolyse them [11,12]. The carbohydrate-binding channels in family 18C proteins are generally formed with the carboxyl terminal residues of the barrel  $\beta$ -strands with their following loops. Although, structurally, the carbohydrate-binding groove is also formed in XAIP, it is severely obstructed by the side-chains of residues Phe13, Pro77, Lys78 and Trp253 (Fig. 5A). The corresponding residues in hevamine are Gly11, Gly81, Ile82 and Trp256 (Fig. 5B). As seen in Fig. 5A, the position of Phe13 in XAIP obstructs the entrance to the carbohydrate-binding groove. It may also be noted that Phe13 is one of the corner residues at the ( $i + 1$ ) position of a tight type I'  $\beta$ -turn conformation, where its side-chain is locked at a distant position from the carbohydrate-binding tunnel and hence cannot be further pushed away by the side-chain of Asp14 at the ( $i + 2$ ) position. Residue Asp14 is further locked at the observed position by the side-chain of Asn12. Furthermore, Asn12 is tightly packed with the side-chain of Tyr256. In view of such a tight packing environment, the orientation of the side-chain of Phe13 is unlikely to change to facilitate interactions with substrates. The residue corresponding to Phe13 is Gly11 in hevamine. Furthermore, Ser49O $\gamma$  in XAIP forms a hydrogen bond with the carbonyl oxygen atom of Gly10, which pushes the loop  $\beta_1$ - $\alpha_1$  into the groove, thus reducing its width considerably. The residue corresponding to Ser49 is Ala47 in hevamine which cannot form a hydrogen bond to create a similar effect. The next most critical

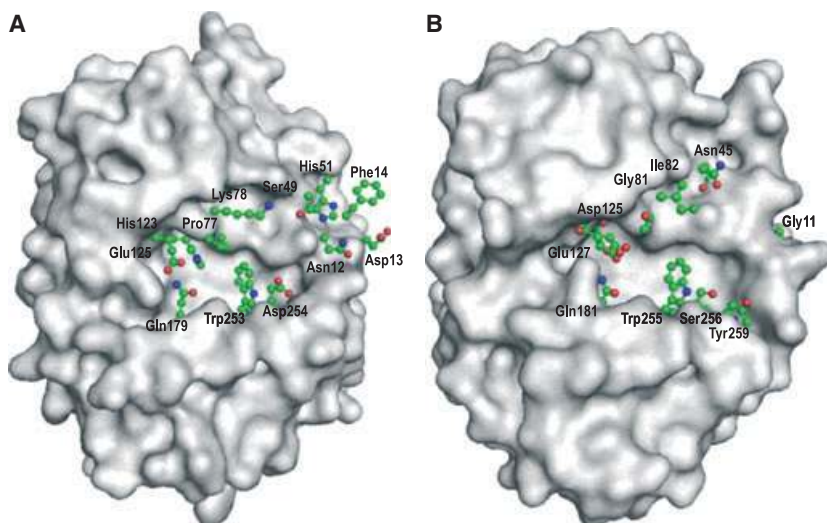


**Fig. 5.** The surface diagrams of XAIP (A) and hevamine (B) showing the carbohydrate-binding channels. The relevant residues oriented towards the centre of the channel are also indicated.

residue in XAIP is Pro77, which further reduces the capacity of the groove for chitin binding as it protrudes into the space of the chitin-binding channel. The corresponding residue in hevamine is Gly81. The closest distance between the atoms of Trp253 from one side of the groove and those of Pro77 from the opposite side of the groove is only 4.1 Å, whereas the corresponding distance in hevamine between Trp255 and Gly81 is 7.7 Å. The side-chain of neighbouring Asp254 is only 3.8 Å away from the side-chain of Trp253 (Asp254 O<sup>δ2</sup>–Trp253 Nε1 = 3.8 Å). Furthermore, Asp254 is locked in a hydrogen-bonded interaction with Trp257 through Asp254 Oδ1 and Trp257 N. The upstream region of the groove is blocked by several other intragroove interactions. The distance between Trp253 C<sup>β</sup> and Tyr181 OH is 3.7 Å, whereas OH is hydrogen bonded to Gln179 (Tyr181 OH...Gln179 O<sup>ε1</sup> = 3.1 Å). The observed interactions involving Trp253 show that the side-chain of Trp253 is absolutely locked at the observed position, and hence is unlikely to change to accommodate the substrates. This means that the size of the carbohydrate-binding channel is not only reduced in width, but is also terminated at the subsite just before the scissile bond. There is another residue, Lys78 (Ile82 in hevamine), which also contributes to the shrinkage of the width of the carbohydrate-binding groove because it interacts with Asp47 through an extremely tight network of water molecules in the centre. Overall, both the length and width of the carbohydrate-binding groove are considerably reduced in XAIP (Fig. 5A) and may not accommodate chitin molecules. Therefore, the so-called substrate-binding site in XAIP is structurally unsuitable for binding to chitin polymers, unlike those of hevamine and other chitinases [10,16,26]. It should be

noted that the structural determination using crystals of XAIP soaked in a solution containing cellobiose revealed the presence of one molecule of cellobiose in the structure. However, as seen in Fig. 6, it was found at the interstitial site away from the so-called carbohydrate-binding site, indicating that XAIP lacks carbohydrate-binding capacity.

### Comparison with the structure of XIP-I

Recently, the structure of XIP-I has been reported [14]. It binds to two types of xylanase from the subgroup of family 18C proteins: GH10 and GH11 xylanases. The overall scaffolding of XAIP is similar to that of XIP-I with an rms shift of 1.3 Å for the C<sup>α</sup> atom positions, showing notable differences observed in the loop regions only. The structural differences are particularly significant in the loops β3–α3 (residues 75–85), α3–β4 (residues 102–112), β4–α4 (residues 124–132), α4–β5 (residues 145–150) and β6–α6 (residues 182–192). An rms shift calculated for the C<sup>α</sup> atoms of these loops, consisting of a total of 48 residues, is approximately 2.1 Å. The loop β3–α3 contributes mainly to the structuring of the carbohydrate-binding groove. A comparison of the conformation of the β3–α3 loop of XAIP with the corresponding loop in XIP-I shows that the loop in XAIP is considerably more rigid as a result of the presence of two Pro residues at positions 77 and 80. The corresponding residues in XIP-I are Tyr80 and Gly83, respectively. This loop forms a part of the boundary wall of the sugar-binding groove. The next important loop α4–β5 in XIP-I is reported to be involved in the binding to GH11 xylanase, whereas the corresponding loop in XAIP is shorter in length by three residues (Fig. 1). It also lacks crucial residues,

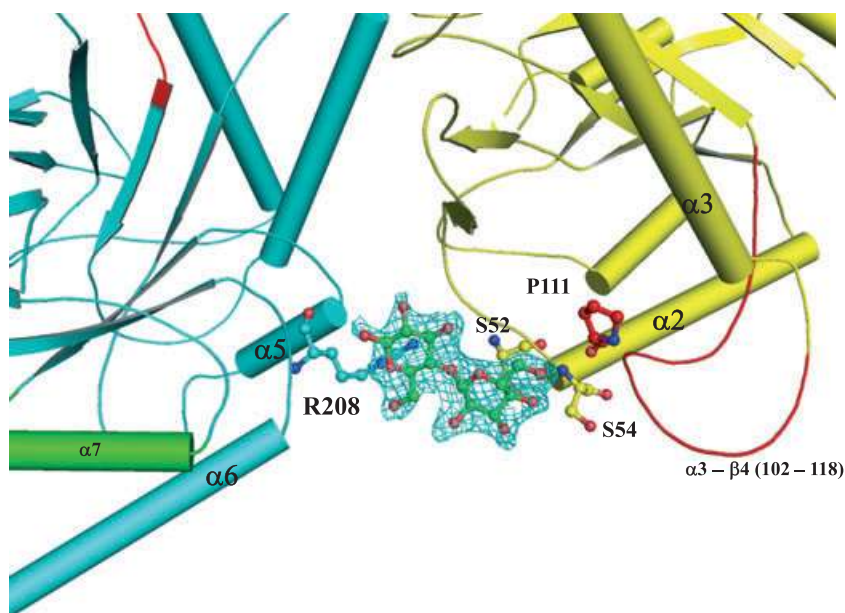


**Fig. 6.** The initial  $|F_o - F_c|$  electron density for cellobiose at  $2.5\sigma$  as located between two symmetry-related molecules of XAIP.

such as Arg and Lys, that interact preferentially with xylanase. Furthermore, this loop in XAIP forms a structure with a rigid type I  $\beta$ -turn conformation, as a result of which it lacks conformational adaptability with respect to the substrate-binding cleft of the xylanase molecule. However, a neighbouring loop  $\alpha 3$ – $\beta 4$  in XAIP appears to be chemically and structurally suitable for binding in the cleft of GH11 xylanase, because this loop in XAIP is relatively long and has a flexible conformation (Fig. 7A). Therefore, it fits into the substrate-binding cleft of GH11 xylanase very well and results in the formation of several interactions between the two proteins (Fig. 7B). On the other hand, the corresponding loop in XIP-I is shorter in length and has a structure with a rigid type I  $\beta$ -turn conformation; therefore, its adaptability is restricted and hence it is not observed in the substrate-binding cleft of GH11 xylanase. The roles of neighbouring loops  $\alpha 3$ – $\beta 4$  and  $\alpha 4$ – $\beta 5$  in the structures of XAIP and XIP-I seem to have interchanged for the interactions with GH11 xylanase. In addition, the residues from the N-terminal side of  $\alpha$ -helix  $\alpha 2$  also interact with xylanase. The second binding site reported in the structure of XIP-I is located on the opposite surface of the protein in which residues of helix  $\alpha 7$  are mainly responsible for binding to another class of xylanase GH10. In contrast, the residues of helix  $\alpha 7$  in XAIP are unable to interact with xylanase GH10 because of the steric hindrance caused by the presence of a neighbouring enlarged loop  $\beta 6$ – $\alpha 6$  (Fig. 7C). This loop in XAIP has three extra residues relative to that of XIP-I (Fig. 1), and the tip of the loop adopts a highly rigid type III  $\beta$ -turn

conformation. It protrudes into the solvent from the protein surface, which may hamper the interactions between residues of  $\alpha 7$  and those of GH10 because of steric hindrance. On the other hand, it has been shown by solution studies that XAIP inhibits the activity of  $\alpha$ -amylase in a 1 : 1.2 molar ratio. The inhibition of  $\alpha$ -amylase by XAIP was also observed in the presence of GH11 xylanase. Thus, the inhibition of  $\alpha$ -amylase by XAIP is unaffected by the addition of GH11 xylanase. As mentioned above, it appears that this side of the protein with helix  $\alpha 7$  and loop  $\beta 6$ – $\alpha 6$  is not suitable for binding to xylanase GH10, as observed in XIP-I, but seems to be an appropriate motif for binding with GH13  $\alpha$ -amylase. It is noteworthy that the residues of loop  $\beta 6$ – $\alpha 6$ , consisting of Ser187–Tyr188–Ser189–Ser190–Gly191–Asn192, create a favourable condition for interactions with the residues considered to be indicative of true  $\alpha$ -amylase [27,28] (Fig. 7C). As observed in the case of the  $\alpha$ -amylase–BASI complex (BASI, barley  $\alpha$ -amylase/subtilisin inhibitor) [27], the  $\beta$ -barrel axis of XAIP is nearly perpendicular to the barrel axis of  $\alpha$ -amylase. The residues of  $\alpha$ -helix  $\alpha 7$  and the loop  $\beta 6$ – $\alpha 6$  form extensive interactions with the residues of the V-shaped binding cleft of  $\alpha$ -amylase. There are at least 12 hydrogen bonds and several van der Waals' contacts ( $\leq 4.0$  Å) between the two molecules. There are at least six common residues of  $\alpha$ -amylase that participate in the formation of hydrogen bonds with BASI and XAIP, indicating a significantly similar mode of binding. Thus, it can be stated unambiguously that XAIP inhibits the actions of enzymes GH11 xylanase and GH13  $\alpha$ -amylase,

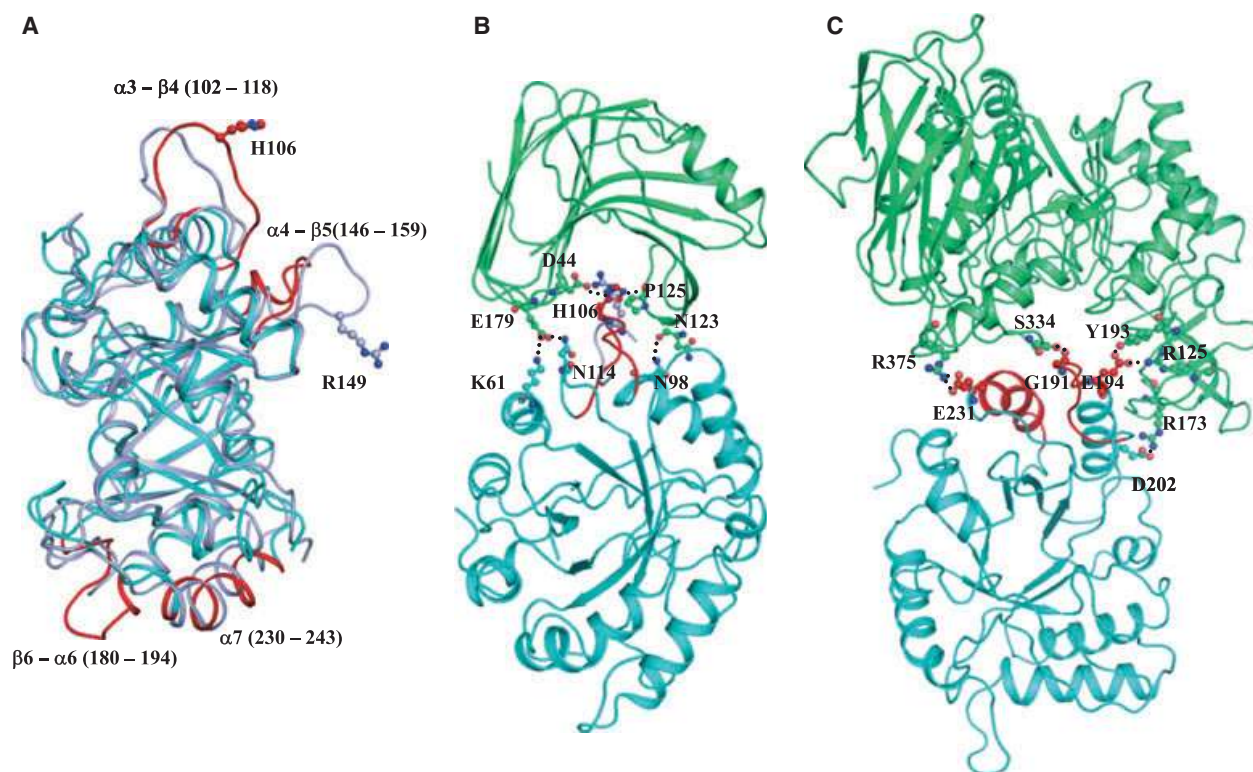


**Fig. 7.** (A) Superimposed loops  $\alpha 3$ - $\beta 4$ ,  $\alpha 4$ - $\beta 5$ ,  $\beta 6$ - $\alpha 6$  and helix  $\alpha 7$  of XAIP (cyan) and XIP-I (sky blue) (Protein Data Bank code: 1TE1). The key residues involved in interactions with GH11 xylanase are also shown in the respective molecules. (B) XAIP (cyan) is shown to interact with GH11 xylanase (green) through loops  $\alpha 3$ - $\beta 4$  (residues 102-118) (red). Also shown is the loop  $\alpha 4$ - $\beta 5$  (sky blue) of XIP from the structure of its complex with GH11 xylanase (Protein Data Bank code: 1TE1(9)). (C) XAIP (cyan) is shown to interact with  $\alpha$ -amylase (green) through  $\alpha$ -helix  $\alpha 7$  (residues 230-243) and loop  $\beta 6$ - $\alpha 6$  (residues 180-194).

whereas XIP-I inhibits the functions of GH11 and GH10 xylanases.

## Discussion

As indicated by enzyme assay, extracellular secretory XAIP lacks chitin hydrolysing activity. However, biochemical assays with various common pathogen enzymes have shown that XAIP inhibits the enzymatic actions of GH11 xylanase and GH13  $\alpha$ -amylase separately, as well as simultaneously. These observations show that XAIP possesses two independent binding sites. In this regard, XAIP appears to be functionally different from other members of the family 18C proteins: hevamine, Con-B and narbonin. In contrast, it resembles closely XIP-I, which has been shown to possess two independent binding sites for two structurally different GH10 and GH11 xylanases. The two binding sites have been shown to coexist independently and are located distantly on the opposite ends of the elliptical XIP-I molecule [9,14]. The comparison of XAIP with XIP-I indicates that both proteins possess two

independent binding sites on a similarly folded TIM barrel structure. One of the two sites of XAIP, as in the XIP-I molecule, is involved in the inhibition of GH11 xylanase. This site in XIP-I consists of a  $\pi$ -shaped flexible loop,  $\alpha 4$ - $\beta 5$ , which is easily inserted into the binding cleft of GH11 xylanase. The corresponding loop in XAIP is considerably shorter in length as a result of three deletions (Fig. 1), and adopts a rigid structure with a type I  $\beta$ -turn conformation in the middle of the short loop, making it unsuitable for binding in the wide binding cleft of GH11 xylanase. However, there exists another loop  $\alpha 3$ - $\beta 4$  in the vicinity of loop  $\alpha 4$ - $\beta 5$  which possesses the required chain length, with a flexible conformation and chemically suitable amino acid residues. Docking studies have also indicated that it fits well into the substrate-binding cleft of GH11 xylanase by laterally moving it along the interface, and extensive intermolecular interactions are formed between the residues of loop  $\alpha 3$ - $\beta 4$  and  $\alpha$ -helix  $\alpha 2$  of XAIP with the residues of the cleft of GH11 xylanase. In contrast, in the case of XIP-I, the residues involved in the interaction with GH11

xylanase belong mainly to the loop  $\alpha 4$ – $\beta 5$  and the C-terminal end of  $\alpha$ -helix  $\alpha 2$ . The buried surface area in the interface between XAIP and GH11 xylanase is  $1206 \text{ \AA}^2$ . The corresponding buried surface area for XIP-I and GH11 xylanase was calculated to be  $1635 \text{ \AA}^2$  [9]. The second binding site in XIP-I is observed on the opposite face of the protein, which is involved in the inhibition of xylanase GH10. The residues involved are mainly from helix  $\alpha 7$  which interacts extensively with the residues of the binding site of the folded TIM barrel structure of xylanase GH10. The superimposition of XAIP on XIP-I reveals that XAIP cannot bind to xylanase GH10 because of steric hindrance caused by an outwardly protruding loop,  $\beta 6$ – $\alpha 6$ , which is located on the same face of the protein in which helix  $\alpha 7$  is present. In striking contrast, the corresponding loop in XIP-I is considerably shorter because of four deletions (Fig. 1), does not extend outwardly from the body of the protein and hence does not cause steric problems in the binding site of xylanase GH10. However, the face containing loop  $\beta 6$ – $\alpha 6$  and  $\alpha$ -helix  $\alpha 7$  in XAIP was found to be highly compatible with the binding site of GH13  $\alpha$ -amylase. Solution studies have shown that XAIP inhibits  $\alpha$ -amylase, and docking studies have provided very good fitting between the surface containing  $\alpha$ -helix  $\alpha 7$  and loop  $\beta 6$ – $\alpha 6$  of XAIP and the binding site of GH13  $\alpha$ -amylase. The residues of XAIP that interact with  $\alpha$ -amylase belong mainly to the loop  $\beta 6$ – $\alpha 6$  and helix  $\alpha 7$ . This clearly shows that XAIP forms extensive interactions with  $\alpha$ -amylase through this favourable interface between two proteins. It is noteworthy that the residues of  $\alpha$ -amylase not only interact through helix  $\alpha 7$ , but also form several additional interactions with residues of the  $\beta 6$ – $\alpha 6$  loop. A comparison of the  $\alpha$ -amylase binding surface of XAIP with those of other members of the subgroup, XIP-I, hevamine, Con-B and narbonin, shows a significant similarity, indicating that these proteins may also be involved in the inhibition of  $\alpha$ -amylase. The total buried surface area in the interface between XAIP and  $\alpha$ -amylase is about  $1347 \text{ \AA}^2$ , which is considerably less than the value of  $2355 \text{ \AA}^2$  reported for the BASI and  $\alpha$ -amylase interface [29]. However, this correlates well with the observed binding constants, the values of which for XAIP– $\alpha$ -amylase and BASI– $\alpha$ -amylase are  $3.6 \times 10^{-6}$  and  $3.1 \times 10^{-9} \text{ M}$  [30], respectively. In contrast, the corresponding surface in XIP-I is considerably different as the size and conformation of loop  $\beta 6$ – $\alpha 6$  do not overlap. However, it has been shown that XIP-I also inhibits  $\alpha$ -amylase activity relatively poorly [31], because the intended binding site in XIP-I is less favourably oriented for binding to  $\alpha$ -amylase. In this regard, the

corresponding sites in hevamine, Con-B and narbonin differ from the binding site in XAIP because the loops  $\alpha 3$ – $\beta 4$  and  $\alpha 4$ – $\beta 5$  are of inconsistent sizes. Therefore, these may bind to either a different enzyme or to GH11 xylanase with low affinity. Although XAIP lacks chitinase activity, its sequence and structural features are closely related to chitinases in the GH18 family [10]. It is well known that plant chitinases work as defence proteins against bacterial and fungal infections. In addition, it has been shown previously that plant chitinases are induced on pathogen infection and are classified as pathogenesis-related proteins [32].

## Experimental procedures

### Purification of XAIP

The samples of underground bulbs of *S. multiflorus* were collected from local nurseries. The bulbs were cut into small pieces and pulverized in the presence of liquid nitrogen in a ventilated hood. The pulverized plant tissues were stirred for 24 h at  $4 \text{ }^\circ\text{C}$  in the extraction solution containing 50 mM phosphate buffer, 0.2 M sodium chloride, pH 7.2; 2.5 g of polyvinylpyrrolidone per 100 mL were added to the sample at the time of homogenization. The homogenate obtained was centrifuged at  $5000 \text{ g}$  for 30 min at  $4 \text{ }^\circ\text{C}$ . The supernatant was loaded onto a DEAE–Sephadex A-50 column ( $50 \times 2 \text{ cm}$ ) which was equilibrated with 50 mM phosphate buffer, pH 7.2. The protein was eluted using a continuous gradient of 0.0–0.5 M NaCl in 50 mM phosphate buffer, pH 7.2. The second peak of the eluted solution was pooled and gel filtrated using a Sephadex G-50 column ( $150 \times 1 \text{ cm}$ ) with 25 mM Tris/HCl, pH 8.0, at a flow rate of  $6 \text{ mL}\cdot\text{h}^{-1}$ . The first peak was collected, pooled and lyophilized. In a separate experiment, the bulb tissues were crushed and insoluble material was removed using simple filtration with a very fine cloth. The filtered samples were subjected to ammonium sulfate precipitation and XAIP was purified from the precipitant. The sequence of the first 20 amino acid residues from the N-terminus was determined using an automatic protein sequencer PPSQ21A (Shimadzu, Kyoto, Japan).

### Estimation of XAIP in different tissues

In order to examine the tissue distribution of XAIP in *S. multiflorus*, equal amounts of tissues from root, germinated bulb, leaf and flower were homogenized separately with five-fold (w/v) phosphate buffer in a mortar and pestle, and left to stand for 6 h at  $4 \text{ }^\circ\text{C}$ . After centrifugation, the supernatants of all four tissues were concentrated separately. These were desalted and SDS–PAGE for all four samples was run. In addition,  $20 \text{ }\mu\text{L}$  of each sample was used to test the inhibitory activity of XAIP against GH11

xylanase and GH13  $\alpha$ -amylase enzymes. Furthermore, the subcellular localization of XAIP was also obtained using the reliable prediction procedures of BACELLO [20], CELLO [21] and PROT COMP VERSION 6.0 [22]. The procedures used signal peptide, nucleotide and amino acid sequences for this protein. All three procedures gave a very high percentile for this protein to be extracellular.

### Complete nucleotide sequence determination

In order to obtain the complete amino acid sequence of XAIP, fresh tissue from bulbs of *S. multiflorus* was used. It was homogenized in 4 M guanidine isothiocyanate (GITC) buffer (pH 5.0) in ice-cooled conditions and stored at  $-70^{\circ}\text{C}$ . Total RNA was extracted by the phenol–chloroform method [33]. Poly(A<sup>+</sup>) mRNAs were isolated from total RNA using an oligo(dT) cellulose column (Amersham Pharmacia Biotech, Piscataway, NJ, USA). The small syringe column packed with oligo(dT) cellulose was washed with 10 mL of high-salt buffer (1 M NaCl), 1 mM Na<sub>2</sub>-EDTA, 40 mM Tris/HCl. Total RNA was mixed with an equal volume of salt 1 buffer, warmed to  $65^{\circ}\text{C}$  and cooled immediately by placing it on ice. The chilled RNA was passed through the column packed with oligo(dT) cellulose. The column was washed with 3 mL of low-salt buffer (0.1 M NaCl, 1 mM Na<sub>2</sub>-EDTA). Amplification was carried out with Moloney Murine Leukaemia Virus reverse transcriptase polymerase using oligo(dT) primers. A portion (2  $\mu\text{L}$ ) of the reverse transcriptase-polymerase chain reaction (RT-PCR) was used for PCR amplification of the gene. The primers were designed using already determined N-terminal sequences and based on the sequence obtained from the preliminary structural analysis. Both forward and reverse primers were synthesized. The degenerate primers were used to amplify the gene. The forward primer 5'-GCNAAYYTNGAYATHGCNGT-3' was prepared from the known amino acid sequence of Ala–Asn–Leu–Asp–Ile–Ala–Val, which was obtained using automatic sequencing from Edman degradation [34]. The reverse primer 5'-CCANCCYTCNCCNARDAYTT-3' was degenerated from the amino acid residues Lys–Ile–Leu–Gly–Glu–Gly–Trp, as obtained from the structural determination with characteristic electron densities for these residues. PCRs were carried out with Taq polymerase (Promega, Madison, WI, USA) using an MJ Research thermal cycler model PTC-100 (Watertown, MA, USA). The complete nucleotide sequence of XAIP was determined using cloned double-strand DNA (pGEM-T) with automatic sequencer model ABI-377 (Foster City, CA, USA).

### Chitinolytic activity assay

As XAIP showed a maximum sequence identity of 48% with the chitin hydrolysing protein hevamine, its activity as a chitinase enzyme was examined. Chitin azure (chitin dyed with Remazol Brilliant violet 5R) was procured from

Sigma-Aldrich (St Louis, MO, USA). The chitinase enzyme from *Streptomyces griseus* was also obtained from Sigma-Aldrich. Substrate chitin azure (2.5 mg·mL<sup>-1</sup>) was dissolved in sodium acetate buffer, pH 5.5, and in another buffer at pH 8.0; 250  $\mu\text{L}$  of 1  $\mu\text{M}$  and 100  $\mu\text{M}$  XAIP were added and the solution was incubated at  $37^{\circ}\text{C}$ . Similar set-ups were prepared with chitinase and with the buffer alone for use as positive and negative controls, respectively. The mixtures from these set-ups were centrifuged at 1816 g, and the absorbances of the supernatants were recorded at 575 nm at intervals of 2 h.

### Xylanase inhibition assay

Xylanase from *P. furniculosum* and beechwood xylan were purchased from Sigma-Aldrich. The xylanase activity assay was performed using beechwood xylan as a substrate for xylanase enzyme from *P. furniculosum* in 10 mM sodium acetate buffer, pH 5.5; 0.5 mL of substrate (10 mg·mL<sup>-1</sup>) was added to prepare a reaction mixture of 1 mL, containing 5  $\mu\text{M}$  of xylanase, and incubated for 30 min at  $50^{\circ}\text{C}$ . Xylanase acted on the substrate to release the reducing sugar, which was determined by its reaction with dinitrosalicylic acid at 540 nm. The xylan hydrolysing activity of xylanase was determined in the presence of increasing concentrations of XAIP. The percentage of xylanase inhibitory activity was calculated from the residual xylanolytic activity. It was also used to obtain the IC<sub>50</sub> value of XAIP. Each set of experiments was repeated six times with a standard error of  $\leq 2\%$ .

### Amylase inhibition assay

Amylase inhibition by XAIP was determined using  $\alpha$ -amylase from *B. licheniformis* and barley (Sigma-Aldrich); 2  $\mu\text{M}$  of enzyme was incubated with 3.6  $\mu\text{M}$  of XAIP for 10 min at  $37^{\circ}\text{C}$ , sufficient to achieve equilibrium; 1% starch solution (prepared in 50 mM sodium phosphate buffer, pH 7.2) was used to estimate the inhibition by XAIP based on the amount of reducing sugars released by the enzyme in the presence of XAIP. The amount of reducing sugar was estimated by dinitrosalicylic acid based on the Bernfeld method [35]. The concentration of XAIP needed to reduce the amylase activity by 50% was calculated from the activity–XAIP concentration curve. The curves were fitted using Sigma plot software, and the IC<sub>50</sub> value of XAIP was calculated using varying concentrations ranging from 0.6 to 4.8  $\mu\text{M}$ . All spectroscopic measurements were made using a UV–visible spectrophotometer (Lambda 25; Perkin-Elmer, Boston, MA, USA) at 540 nm. Each set of experiments was repeated six times with an estimated standard error of  $\leq 3\%$ .

In order to examine complex formation between XAIP ( $M_w = 30$  kDa) and xylanase ( $M_w = 20$  kDa), gel filtration of the mixture of XAIP and GH11 xylanase was carried out. XAIP and xylanase were mixed in a 1 : 1 molar

ratio in 10 mM sodium acetate buffer at pH 5.5 to give a final protein concentration of 20 mg·mL<sup>-1</sup>. It was passed through a Sephadex G-100 gel filtration column (100 × 2 cm) using 25 mM Tris/HCl, pH 8.0, at a flow rate of 6.0 mL·h<sup>-1</sup>. The elution profile showed the presence of three peaks, with peak 1 being the major fraction. The estimation of the molecular weight indicates a first peak of approximately 50 kDa, a second peak of 30 kDa and a third peak of about 20 kDa. A similar gel filtration experiment was also carried out for the complex of XAIP with  $\alpha$ -amylase. A mixture of XAIP and  $\alpha$ -amylase was dissolved in 50 mM sodium acetate buffer at pH 7.2 to give a final protein concentration of 20 mg·mL<sup>-1</sup>. It was passed through a Sephadex G-150 gel filtration column (100 × 2 cm) using 25 mM Tris/HCl at a flow rate of 6.0 mL·h<sup>-1</sup>. The elution profile consisted of one main peak and two minor peaks. The molecular weight as estimated from the void volume corresponded to 83 kDa for the main peak. The minor peaks were observed at molecular weights of 53 and 30 kDa, corresponding to the molecular weights of the individual proteins  $\alpha$ -amylase and XAIP, respectively. A further gel filtration experiment with a 1 : 1 : 1 mixture of XAIP, GH11 xylanase and  $\alpha$ -amylase was carried out with a Sephadex G-200 gel filtration column (100 × 2 cm) using 50 mM Tris/HCl buffer at pH 8.0. The elution profile showed a prominent peak at a molecular weight of approximately 103 kDa with five other minor peaks of lower molecular weights.

### Crystallization of XAIP

The freshly purified samples of protein were dissolved in 20 mM phosphate buffer, pH 7.2, to a final protein concentration of 20 mg·mL<sup>-1</sup>. The protein was crystallized by the hanging drop vapour diffusion method at 293 K using 24-well Limbro crystallization plates (Flow Laboratories, McLean, VA, USA). The protein drops of 10  $\mu$ L were equilibrated against reservoir solution containing 0.1 M ammonium sulfate, 20 mM phosphate buffer, pH 7.2, 0.1 M sodium acetate and 20% PEG-6000. The crystals grew to maximum dimensions of 0.3 × 0.15 × 0.10 mm<sup>3</sup> within 3 weeks. The crystals of XAIP were also soaked in three separate reservoir solutions containing sugars [(a) mannose; (b) cellobiose; and (c) *N*-acetylglucosamine] at concentrations in excess of 20 mg·mL<sup>-1</sup>. Attempts were also made to cocrystallize XAIP with the above three sugars.

### Data collection and processing

A complete dataset was collected using a MAR 345 imaging plate scanner (Marresearch, Nordersledt, Germany) mounted on a Rigaku RU-300 rotating anode X-ray generator (Rigaku, Tokyo, Japan) operating at 100 mA and 50 kV. Osmic Blue confocal optics were used to focus Cu K $\alpha$  radiation. The X-ray intensity data were also collected on soaked crystals. The data were indexed and scaled using the

programs DENZO and SCALEPACK [36]. The overall value of  $R_{\text{sym}}$  was found to be 6.5% for the entire dataset on the native crystals. The details of data collection and statistics are summarized in Table 1. The data were also collected on three soaked crystals and three cocrystallized crystals.

### Structural determination

The structure of XAIP has been determined by the molecular replacement method using MOLREP [37]. The coordinates

**Table 1.** Data collection and refinement statistics. Numbers in parentheses correspond to the data in the highest resolution shell.

	Structure of XAIP	Structure of the complex of XAIP and cellobiose
Space group	<i>P</i> 2 <sub>1</sub>	<i>P</i> 2 <sub>1</sub>
Unit cell dimensions		
<i>a</i> (Å)	42.8	42.8
<i>b</i> (Å)	65.4	65.6
<i>c</i> (Å)	49.4	49.4
$\beta$ (deg)	102.0	102.1
Number of molecules in the unit cell	2	2
Resolution range (Å)	48.2–2.0 (2.10–2.07)	48.2–2.0 (2.49–2.40)
Total number of measured reflections	102496	70854
Number of unique reflections	16787 (1239)	10289 (1021)
$R_{\text{sym}}^a$ (%)	6.5 (26.2)	9.1 (33.2)
$I/\sigma(I)$	9.0 (2.1)	5.8 (2.0)
Completeness of data (%)	100 (99.9)	98 (98)
$R_{\text{crist}}^b$ (%)	15.1 (21.8)	19.8 (24.6)
$R_{\text{free}}^c$ (%)	18.6 (28.7)	21.4 (27.5)
Protein atoms	2108	2108
Water oxygen atoms	300	115
Phosphate ion	1	1
Acetate	1	1
Rmsd in bond lengths (Å)	0.01	0.01
Rmsd in bond angles (deg)	1.8	2.0
Rmsd in torsion angles (deg)	19.2	26.1
Average <i>B</i> factors (Å <sup>2</sup> )		
Main chain atoms	22.8	33.9
Side-chain and water atoms	29.7	35.5
All atoms	26.5	34.7
Ramachandran's $\phi$ , $\psi$ map, residues in (%)		
Most favoured regions (%)	88.5	91.6
Additionally allowed regions (%)	10.6	7.1
Generously allowed regions (%)	0.9	1.3
Protein Data Bank ID	3HU7	3M7S

<sup>a</sup>  $R_{\text{sym}} = \sum_{hkl} \sum_i |I(hkl) - \langle I(hkl) \rangle| / \sum_{hkl} \sum_i I(hkl)$ . <sup>b</sup>  $R_{\text{crist}} = \sum_{hkl} |F_{\text{obs}}(hkl) - kF_{\text{cal}}(hkl)| / \sum_{hkl} |F_{\text{obs}}(hkl)|$ . <sup>c</sup> 5% of reflections were excluded from refinement and used for the calculation of  $R_{\text{free}}$ .

of the structure of hevamine, which shows a sequence identity of 48%, were used as a model (Protein Data Bank code: 2HVM) [11]. The rotation and transition search functions were computed using reflections in the resolution range 20.0–4.0 Å. This yielded a clear solution with a distinct peak. The molecular packing in the unit cell, calculated using the above solution, did not produce unfavourable short contacts. The transformed coordinates were subjected to 25 cycles of rigid body refinement with REFMAC5 [38] from the CCP4i V4.2 program package [39]. After the first round of refinement, the  $R_{\text{cryst}}$  and  $R_{\text{free}}$  factors reduced to 0.326 and 0.412, respectively (5% of the reflections were used for the calculation of  $R_{\text{free}}$ ). The  $|2F_o - F_c|$  Fourier and  $|F_o - F_c|$  difference Fourier maps computed at this stage clearly indicated new electron densities for at least three loop regions into which the protein chain was built. Further rounds of refinements with these additional protein segments converged  $R_{\text{cryst}}$  and  $R_{\text{free}}$  factors to 0.248 and 0.278, respectively. The manual model building was carried out with graphics programs o [40] and COOT [41] on a Silicon Graphics O2 Workstation. The  $|F_o - F_c|$  difference Fourier map calculated at this stage revealed the positions of one phosphate and one acetate ion. The positions of 300 water oxygen atoms were also determined using ARP/WARP. The refinement finally converged with  $R_{\text{cryst}}$  and  $R_{\text{free}}$  factors of 0.151 and 0.186, respectively. The final refinement statistics are included in Table 1. The structures were also refined using data from the three soaked and three cocrystallized crystals. However, the interpretable electron density was observed only from the data obtained from the soaked crystals with cellobiose (Fig. 6). Therefore, the details of data collection and refinement statistics were included in Table 1 for the structure containing cellobiose only.

### In silico docking

As the biochemical studies indicated specific binding of XAIP with GH11 xylanase and  $\alpha$ -amylase, the interactions between XAIP and  $\alpha$ -amylase and between XAIP and GH11 xylanase were examined using docking procedures. For this purpose, discovery Studio 2.0, INSIGHT II and o program [40] packages were used for docking and structural analysis. The coordinates of a bacterial GH11 xylanase from *P. furniculosum* complexed with XIP-I (Protein Data Bank code: 1TE1) and those of  $\alpha$ -amylase from *B. licheniformis* (Protein Data Bank code: 1BLI) were used separately for docking on the surface of XAIP. Using program o on a silicon graphics workstation O2, the intermolecular interactions between participating molecules involving residues at the interface were optimized. Various sites in the structure of XAIP were examined by docking the molecules of  $\alpha$ -amylase and GH11 xylanase, but the sites that fitted the best were selected. The complexes of XAIP with selected sites were examined to evaluate the intermolecular

interactions between the pairs of proteins, XAIP- $\alpha$ -amylase and XAIP-GH11 xylanase.

### Acknowledgements

The authors acknowledge a grant from the Department of Science and Technology (DST), New Delhi, India. TPS thanks the Department of Biotechnology, Ministry of Science and Technology, New Delhi, India, for the award of Distinguished Biotechnologist. NS and MS thank the Council of Scientific and Industrial Research, New Delhi, India, for the award of Senior Associateships. NS thanks DST for financial assistance under the Fast Track Scheme.

### References

- Juge N (2006) Plant protein inhibitors of cell wall degrading enzymes. *Trends Plant Sci* **11**, 359–367.
- Lebeda A, Luhova L, Sedlarova M & Jancova D (2001) The role of enzymes in plant–fungal pathogen interactions. *Z Pflanzenk Pflanzens J Plant Dis Prot* **108**, 89–111.
- Misas-Villamil JC & van der Hoorn RA (2008) Enzyme–inhibitor interactions at the plant–pathogen interface. *Curr Opin Struct Biol* **11**, 380–388.
- Bugbee WM (1993) A pectin lyase inhibitor protein from cell-walls of sugar-beet. *Phytopathology* **83**, 63–68.
- Mclauchlan WR, Garcia-Conesa MT, Williamson G, Roza M, Ravestein P & Maat J (1999) A novel class of protein from wheat which inhibits xylanases. *Biochem J* **338**, 441–446.
- Gebruers K, Brijs K, Courtin CM, Fierens K, Goesaert H, Rabijns A, Raedschelders G, Robben J, Sansen S, Sorensen JF *et al.* (2004) Properties of TAXI-type endoxylanase inhibitors. *Biochim Biophys Acta* **1696**, 213–221.
- Matteo AD, Bonivento D, Tsernoglou D, Federici L & Cervone F (2006) Polygalacturonase-inhibiting protein (PGIP) in plant defence: a structural view. *Phytochemistry* **67**, 528–533.
- Matteo AD, Giovane A, Raiola A, Camardella L, Bonivento D, De Lorenzo G, Cervone F, Bellincampi D & Tsernoglou D (2005) Structural basis for the interaction between pectin methylesterase and a specific inhibitor protein. *Plant Cell* **17**, 849–859.
- Payan F, Leone P, Porciero S, Furniss C, Tahir T, Williamson G, Durand A, Manzanares P, Gilbert HJ, Juge N *et al.* (2004) The dual nature of the wheat xylanase protein inhibitor XIP-I: structural basis for the inhibition of family 10 and family 11 xylanases. *J Biol Chem* **279**, 36029–36037.
- Vanscheltina ACT, Hennig M & Dijkstra BW (1996) The 1.8 Å resolution structure of hevamine, a plant

- chitinase/lysozyme, and analysis of the conserved sequence and structure motifs of glycosyl hydrolase family 18. *J Mol Biol* **262**, 243–257.
- 11 Hennig M, Jansson JN, Vanschellinga ACT, Dijkstra BW & Schlesier B (1995) Crystal structure of concanavalin B at 1.65 Å resolution. An ‘inactivated’ chitinase from seeds of *Canavalia ensiformis*. *J Mol Biol* **254**, 237–246.
- 12 Hennig M, Pfeffer-Hennig S, Dauter Z, Wilson KS, Schlesier B & Nong VH (1995) Crystal structure of narbonin at 1.8 Å resolution. *Acta Crystallogr Sect D: Biol Crystallogr* **51**, 177–189.
- 13 Payan F, Flatman R, Porciero S, Williamson G, Juge N & Roussel A (2003) Structural analysis of xylanase inhibitor protein I (XIP-I), a proteinaceous xylanase inhibitor from wheat (*Triticum aestivum* var. Soisson). *Biochem J* **372**, 399–405.
- 14 Kengo K & Haruki N (2003) Protein informatics towards function identification. *Curr Opin Struct Biol* **13**, 396–400.
- 15 Farber GK & Petsko GA (1990) The evolution of  $\alpha/\beta$  barrel enzymes. *Trends Biochem Sci* **15**, 228–234.
- 16 Wilson KS & Vorgias CE (1994) Crystal structure of a bacterial chitinase at 2.3 Å resolution. *Structure* **2**, 1169–1180.
- 17 Hackman RH & Goldberg M (1964) New substrates for use with chitinases. *Anal Biochem* **8**, 397–401.
- 18 Machius M, Declerck N, Huber R & Wiegand G (2003) Kinetic stabilization of *Bacillus licheniformis* alpha-amylase through introduction of hydrophobic residues at the surface. *J Biol Chem* **278**, 11546–11553.
- 19 Elliott GO, McLauchlan WR, Williamson G & Kroon PA (2003) A wheat xylanase inhibitor protein (XIP-I) accumulates in the grain and has homologues in other cereals. *J Cereal Sci* **2**, 187–194.
- 20 Pierleoni A, Martelli PL, Fariselli P & Casadio R (2006) BaCelLo: a balanced subcellular localization predictor. *Bioinformatics* **22**, e408–e416.
- 21 Yu CS, Chen YC, Lu CH & Hwang JK (2006) Prediction of protein subcellular localization. *Proteins: struct. funct. Bioinformatics* **64**, 643–651.
- 22 <http://linux.softberry.com/berry.phtml>? access date: March 10, 2010.
- 23 Davis WI, Leaver-Fay A, Chen BV, Block NJ, Kapral JG, Wang X, Murray WL, Arendall BW, Snoeyink J, Richardson SJ *et al.* (2007) MolProbity: all-atom contacts and structure validation for proteins and nucleic acids. *Nucleic Acids Res* **35**, Web Server issue, W375–W383.
- 24 Ramachandran GN & Sasisekaran V (1968) Conformation of polypeptides and proteins. *Adv Protein Chem* **23**, 283–438.
- 25 Laskowski RA, MacArthur MW, Moss DS & Thornton JM (1993) PROCHECK: a program to check the stereochemical quality of protein structures. *J Appl Crystallogr* **26**, 283–291.
- 26 Rao VH, Guan C & van Roey P (1995) Crystal structure of endo-b-N-acetylglucosaminidase H at 1.9 Å resolution: active-site geometry and substrate recognition. *Structure* **3**, 449–457.
- 27 Vallee F, Kadziola A, Bourne Y, Juy M, Rodenburg KW, Svensson B & Haser R (1998) Barley alpha-amylase bound to its endogenous protein inhibitor BASI: crystal structure of the complex at 1.9 Å resolution. *Structure* **15**, 649–659.
- 28 Stanley D, Farnden FJK & Macrae AE (2005) Plant  $\alpha$ -amylase: functions and role in carbohydrate metabolism. *Biologia (Bratis)* **60**, 65–71.
- 29 Micheelsen PO, Vévodova J, De Maria L, Ostergaard PR, Friis EP, Wilson K & Skjot M (2008) Structural and mutational analyses of the interaction between the barley alpha-amylase/subtilisin inhibitor and the subtilisin savinase reveal a novel mode of inhibition. *J Mol Biol* **380**, 681–690.
- 30 Nielsen PK, Bønsager BC, Berland CR, Sigurskjold BW & Svensson B (2003) Kinetics and energetics of the binding between barley alpha-amylase/subtilisin inhibitor and barley alpha-amylase 2 analyzed by surface plasmon resonance and isothermal titration calorimetry. *Biochemistry* **42**, 1478–1487.
- 31 Sancho AI, Faulds CB, Svensson B, Bartolome B, Williamson G & Juge N (2003) Cross-inhibitory activity of cereal protein inhibitors against alpha-amylases and xylanases. *Biochim Biophys Acta* **1650**, 136–144.
- 32 Legrand M, Kauffmann S, Geoffroy P & Fritig B (1987) Biological function of pathogenesis-related proteins: four tobacco pathogenesis-related proteins are chitinases. *Proc Natl Acad Sci USA* **84**, 6750–6754.
- 33 Chomczynski P & Sacchi N (1987) Single-step method of RNA isolation by acid guanidinium thiocyanate phenol–chloroform extraction. *Anal Biochem* **162**, 156–159.
- 34 Edman P (1949) A method for the determination of amino acid sequence in peptides. *Arch Biochem* **22**, 475.
- 35 Bernfeld P (1955) Amylase alpha and beta. *Methods Enzymol* **1**, 149–158.
- 36 Otwinowski Z & Minor W (1997) Processing of X-ray diffraction data collected in oscillation mode. *Methods Enzymol* **276**, 307–326.
- 37 Vagin A & Taplyakov A (1997) MOLREP: An automated program for molecular replacement. *J Appl Crystallogr* **30**, 1022–1025.
- 38 Murshudov GN, Vagin AA & Dodson EJ (1997) Refinement of protein structures by the maximum likelihood method. *Acta Crystallogr Sect D: Biol Crystallogr* **53**, 240–255.

- 39 Collaborative Computational Project, Number 4 (1994) The CCP4 suite: programs for protein crystallography. *Acta Crystallogr Sect D: Biol Crystallogr* **50**, 760–763.
- 40 Jones TA, Zou J, Cowan SW & Kjeldgaard M (1991) Improved methods for building models in electron density maps and the location of errors in these models. *Acta Crystallogr A* **47**, 110–118.
- 41 Emsley P & Cowtan K (2004) Coot: model-building tools for molecular graphics. *Acta Crystallogr Sect D: Biol Crystallogr* **60**, 2126–2132.
- 42 DeLano WL (2002) *The PyMol Molecular Graphics System*. DeLano Scientific, San Carlos CA. <http://www.pymol.org>. Access date March 17, 2010.